PHYSICAL REVIEW A **79**, 011803(R) (2009)

Degenerate perturbation theory describing the mixing of orbital angular momentum modes in Fabry-Perot cavity resonators

David H. Foster,[1,*] Andrew K. Cook,[2] and Jens U. Nöckel[2]
[1]*Deep Photonics Corporation, Corvallis, Oregon 97333, USA*
[2]*Department of Physics, University of Oregon, Eugene, Oregon 97403, USA*
(Received 28 July 2008; published 8 January 2009)

We present an analytic perturbation theory which extends the paraxial approximation for a common cylindrically symmetric stable optical resonator and incorporates the differential, polarization-dependent reflectivity of a Bragg mirror. The degeneracy of Laguerre-Gauss modes with distinct orbital angular momentum (OAM) and polarization, but identical transverse order N, will become observably lifted at sufficiently small size and high finesse. The resulting paraxial eigenmodes possess two distinct OAM components, the fractional composition subtly depending on mirror structure.

DOI: 10.1103/PhysRevA.79.011803 PACS number(s): 42.50.Tx, 42.60.Da, 42.60.Jf

Polarization-dependent effects in three-dimensional optical systems have in recent years received attention under the aspect of orbital angular momentum (OAM) [1]. It has become important to understand the OAM interactions with interfaces [2,3], waveguides [4], and resonators. One particular mechanism that warrants investigation is that of small corrections to the paraxial theory of resonators giving rise to what may be regarded as optical spin-orbit coupling [5,6].

In this Rapid Communication, we extend electromagnetic resonator theory [7] to provide a complete perturbation analysis and numerical computations for an optical cavity which has an axis of rotational symmetry ($\hat{\mathbf{z}}$), but nevertheless does not conserve the component ℓ of OAM along that axis. This phenomenon itself is remarkable because the model system, shown in Fig. 1(a), approaches the *paraxial* limit in which OAM conservation might be taken for granted. Standard paraxial modes may be chosen to have well-defined ℓ because the polarization is transverse to $\hat{\mathbf{z}}$ and factors out of the wave problem, leaving a scalar Helmholtz equation which maps to a quantum harmonic oscillator [8]. Labeling the resulting transverse spectrum by $\ell \in \mathbb{Z}$ and a radial node number $p \in \mathbb{N}_0$, all modes with the same transverse order $N=2p+|\ell|$ are degenerate in this set of approximations. Therefore, going beyond this theory entails a degenerate perturbation theory for which we construct a coupling Hamiltonian V with the nominal Gaussian divergence angle $\theta_D \equiv kw_0/2$ as its small parameter. Here k is the wave number and w_0 is the waist radius. Since V is typically not diagonal in ℓ, the solutions may be far from ℓ eigenstates. This holds even for arbitrarily small θ_D. Both polarization and ℓ mix in a paraxial spin-orbit coupling [5,6]. Our work, in part, yields a way of generating OAM and other nonuniformly polarized light. Furthermore, in work involving cavity quantum electrodynamics, paraxial theory at the level developed here may be needed to distinguish spectral anticrossings arising from passive cavity physics from those of strong photon-electron coupling.

The main result of our work is an analytical, quantitative expression for the degree of OAM mixing in a dome-shaped cavity with a Bragg mirror. The latter is crucial to achieving high finesse in optical microcavities. Our results also shed light on the recently observed coupling between spatial and polarization degrees of freedom in broad-area vertical-cavity surface emitting lasers [9]: polarization mixing was found to cause surprising spectral complexity even with simple (square) boundaries, accompanied by intricate polarization patterns in the far-field emission. The essential physics is provided by the interaction of differently polarized plane-wave components with the planar, high-reflectivity distributed Bragg reflector (DBR) on which both Ref. [9] and our system in Fig. 1(a) are based.

Typical DBRs comprise dielectric multilayers and have a "form birefringence": the reflectivities for TE (s-polarized) and TM (p-polarized) plane waves, $r_{s(p)}=|r_{s(p)}|\exp(i\phi_{s(p)})$, are unequal in phase at nonzero angles of incidence, θ. Previously [5,10], we had found numerically that the reflection phase difference $\phi_s(\theta_D)-\phi_p(\theta_D)\neq 0$ is responsible for the polarization mixing. A consequence of great practical importance is that by tuning cavity or mirror parameters, the coupling of OAM imposed by Maxwell's equations can be rigorously *turned off* for selected modes, giving them well-defined ℓ. Aside from the consideration of OAM, our perturbation theory is fundamental to paraxial theory itself: we perform a significant extension to and completion of previous work by Yu and Luk [7] which derived the lowest-order corrections to the paraxial modes of two-mirror cavities having perfect electrically conducting mirrors, $r_s=r_p=-1$. Our approach, which allows a more general, dielectric planar mirror, requires the construction of a 2×2 perturbation matrix V and predicts very different results when r_s and r_p are different functions.

The work of Ref. [7] and its precursors (e.g., Ref. [11]) appears to be forgotten in the current literature. This can be attributed to the difficulty of experimentally observing the small spectral splittings caused by slightly nonparaxial perturbations. Agreement with a degenerate perturbation theory for $r_{s(p)}=-1$ was experimentally demonstrated using microwaves [11] where, due to comparable resonator size and wavelength, the mode spacing is large enough to resolve the lifting of the $(N+1)$-fold degeneracies labeled by N. However, with recent progress in miniaturization [12], compa-

*davidhfoster@gmail.com

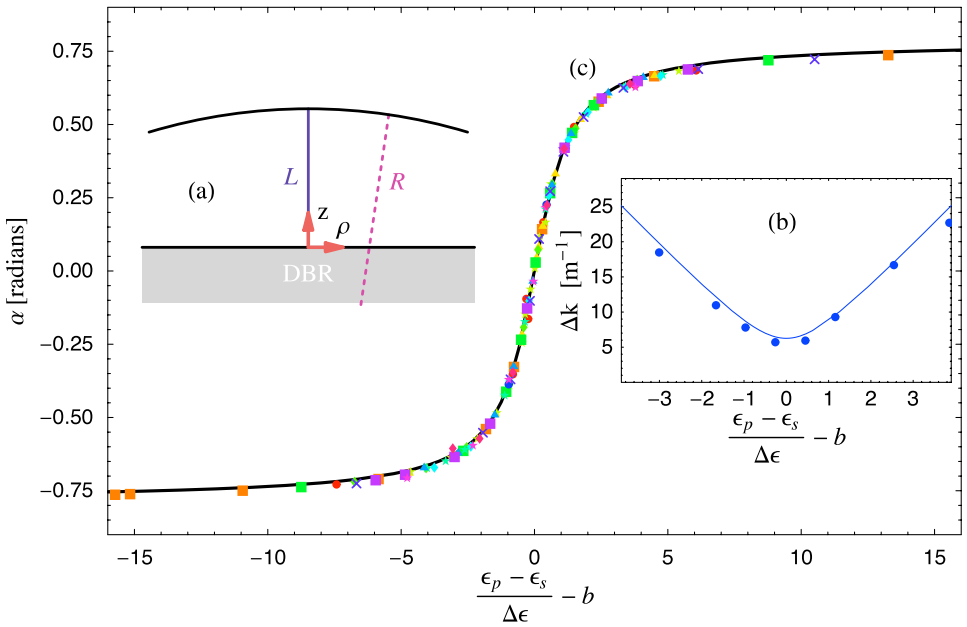

FIG. 1. (Color online) (a) Planoconcave model geometry. The top mirror radius of curvature R is 100 μm in the examples. (b) Wave number splitting $\Delta k \equiv k_2 - k_1 = \delta k_2 - \delta k_1$ from numerical data at $L=25$ μm, $\lambda \approx 400$ nm, indicating the avoided crossing between a mixable pair of modes. (c) Numerical results (symbols) for the mode mixing angle α closely fit the (solid) curve $\alpha = \arctan[(\epsilon_p - \epsilon_s)/\Delta\epsilon - b]/2$. Different symbols (colors) represent data series at $L=2.5-25$ μm (in steps of 2.5 μm) with $kR \approx 780$ to 1631. $\Delta\epsilon$ and b are fit here for each series.

rable size parameters are becoming accessible to optical cavities similar to Fig. 1(a).

To write the splittings described in Ref. [7] in a form we can use for the following discussion, let us first review the unperturbed vector-field basis spanning the Nth transverse multiplet. These are the *Laguerre-Gauss* (LG) modes, written in polar coordinates as a product $M_N^\ell(\rho,\phi,z)\hat{\boldsymbol{\sigma}}_s$ of a scalar part M_N^ℓ, having orbital angular momentum ℓ, and a circular polarization vector $\hat{\boldsymbol{\sigma}}_s \equiv (\hat{\mathbf{x}} + si\hat{\mathbf{y}})/\sqrt{2}$, where $s = \pm 1$ is the spin degree of freedom. Expressions for the LG modes and their Bessel wave decompositions are given in Ref. [13]. Perturbations that preserve rotational symmetry around $\hat{\mathbf{z}}$ will only couple those $M_N^\ell(\rho,\phi,z)\hat{\boldsymbol{\sigma}}_s$ for which the *total angular momentum* $m = \ell + s$ around this axis is the same [13]. We henceforth consider N and m to be fixed, non-negative parameters; we will briefly discuss later the allowance of $m < 0$. The nonconservation of OAM emerges here because s can generally[1] take two values, corresponding to the basis states $M_N^{m-1}\hat{\boldsymbol{\sigma}}_1$ and $M_N^{m+1}\hat{\boldsymbol{\sigma}}_{-1}$. No symmetry prevents these states from coupling, unless $m=0$, in which case time-reversal invariance applies.

Nevertheless, no such OAM coupling is found in Ref. [7], where perturbations merely split the wave numbers of the pair $\{M_N^{m\mp1}\hat{\boldsymbol{\sigma}}_{\pm1}\}$ by an amount

$$\Delta k_{\mathrm{LG}} \equiv k(M_N^{m+1}\hat{\boldsymbol{\sigma}}_{-1}) - k(M_N^{m-1}\hat{\boldsymbol{\sigma}}_1) = \frac{m}{4kLR}. \tag{1}$$

The calculation assumes a dome of vertical length L, top mirror radius of curvature R, and $r_{s(p)} = -1$. We will now show that a more realistic model for $r_{s(p)}$ leads to actual resonator modes $\boldsymbol{\Psi}_{N,m,1}$ and $\boldsymbol{\Psi}_{N,m,2}$ having a given m but forming a rotation of the LG basis pair by a mixing angle $\alpha \in (-\pi/4, \pi/4)$:

$$\begin{pmatrix} \boldsymbol{\Psi}_{N,m,1}(\alpha) \\ \boldsymbol{\Psi}_{N,m,2}(\alpha) \end{pmatrix} = \begin{pmatrix} \cos\alpha & -\sin\alpha \\ \sin\alpha & \cos\alpha \end{pmatrix} \begin{pmatrix} M_N^{m-1}\hat{\boldsymbol{\sigma}}_1 \\ M_N^{m+1}\hat{\boldsymbol{\sigma}}_{-1} \end{pmatrix}. \tag{2}$$

The states at $\alpha = \pm\pi/4$ are *hybrid modes*, one of which is predominantly (though not completely) composed of TM plane waves, the other being predominantly TE [13,14]. This approximate polarization separation of the hybrid modes yields an intuitive picture of mode mixing; the separation acts as a lever arm by which the Bragg mirror, having $\phi_s \neq \phi_p$, rotates the eigenmode basis away from the LG modes and toward the hybrid modes.

The OAM nonconservation described above is exhibited by the paraxial modes of two-mirror axisymmetric cavity resonators which (a) are of sufficiently small size with respect to wavelength, (b) have sufficiently narrow resonance widths (low loss), and (c) have at least one mirror for which $\phi_s \neq \phi_p$ (commercial dielectric mirrors meet this requirement). The first two requirements are essential in splitting the degeneracies of high order Gaussian modes, and Eq. (1) allows us to estimate whether this is possible. To perform the degenerate perturbation theory in the presence of property (c), we first develop the perturbation Hamiltonian V in the two-mode basis $\{M_N^{m\mp1}\hat{\boldsymbol{\sigma}}_{\pm1}\}$. V must be symmetric ($V_{21} = V_{12}$) and, for our purposes, may be taken to be traceless ($V_{22} = -V_{11}$). V then has eigenvectors $\vec{v}_1 = \binom{\cos\alpha}{-\sin\alpha}$ and $\vec{v}_2 = \binom{\sin\alpha}{\cos\alpha}$, with

$$\alpha = (1/2)\arctan(V_{12}/V_{22}), \tag{3}$$

and eigenvalues $\delta k_{1(2)} = \mp(V_{12}^2 + V_{22}^2)^{1/2}$. As system parameters are varied, the elements of V change and an anticrossing of the hybrid modes emerges; cf. Fig. 1(b).

All deviations from the paraxial limit must be considered to lowest order in θ_{D}^2, which for our cavity is $\theta_{\mathrm{D}}^2 = 2/[k\sqrt{L(R-L)}]$. The physical derivation of V is facilitated by noting that in the anticrossing scenario, $\alpha=0$ is equivalent to $V_{12}=0$ and hence corresponds to the assumptions underly-

[1]Specifically, when $N \geq 2$ and $0 < |m| < N+1$, there are two mixable basis states and Eq. (2) applies.

ing the known result Eq. (1). Thus, Eq. (1) should be reproduced by our model at $\alpha=0$. In wave-number units, we therefore set

$$V_{22} = -V_{11} = \frac{1}{2}\Delta k_{\mathrm{LG}} = \frac{m}{16}\sqrt{\frac{L}{R}\left(1-\frac{L}{R}\right)}\frac{\theta_{\mathrm{D}}^2}{L}. \tag{4}$$

Although Eq. (1) was derived for ideal-metal cavities, our more general DBR boundary conditions do not affect Eq. (4), because they shift all LG modes with the same N *equally*. To explain this, consider the *penetration depths* $\delta L_{s(p)}$ of each of $M_N^{m\mp1}\hat{\boldsymbol{\sigma}}_{\pm1}$ into the mirror layers. For a plane wave of s or p polarization with incident angle θ at a DBR, $\delta L_{s(p)} = \phi_{s(p)}(k,\theta)/(2k)$. In order to capture the relevant material properties of the DBR, we neglect transmission and expand its reflection phase in the plane wave angle of incidence, θ, as $\phi_{s(p)}(k,\theta) \approx \phi_0(k) + \epsilon_{s(p)}(k)\theta^2$.

Any vectorial mode $\boldsymbol{\Psi}$ can be decomposed into azimuthally symmetrized plane waves (Bessel waves) by defining a "tilde" operator such that $\tilde{\Psi}^{s(p)}(\theta)$ essentially denotes the amplitudes of the TE (TM) plane waves of polar angle θ. The paraxial $\tilde{\Psi}^{s(p)}(\theta)$ is nonzero only near $\theta\approx0$, with the *averaged* reflection phase of $\boldsymbol{\Psi}$ being

$$\langle\phi\rangle_{\boldsymbol{\Psi}} \equiv \int [|\tilde{\Psi}^s(\theta)|^2\phi_s(\theta) + |\tilde{\Psi}^p(\theta)|^2\phi_p(\theta)]\theta d\theta, \tag{5}$$

with the normalization $\int(|\tilde{\Psi}^s|^2+|\tilde{\Psi}^p|^2)\theta d\theta=1$. Specializing to the LG modes with the abbreviation $\boldsymbol{\Lambda}_{\pm1}\equiv M_N^{m\mp1}\hat{\boldsymbol{\sigma}}_{\pm1}$, circular polarization leads to $|\tilde{\Lambda}^s_{\pm1}(\theta)|^2=|\tilde{\Lambda}^p_{\pm1}(\theta)|^2$. The harmonic-oscillator nature of the transverse field [8] entails that Eq. (5), with the above expansion for $\phi_{s(p)}$, depends only on the mode order N, but not on ℓ. This carries over to the average penetration depth $\langle\delta L\rangle_{\boldsymbol{\Lambda}_{\pm1}}=\langle\phi\rangle_{\boldsymbol{\Lambda}_{\pm1}}/(2k)$, and hence the effective cavity length $L+\langle\delta L\rangle_{\boldsymbol{\Lambda}_{\pm1}}$ is identical for both modes $\boldsymbol{\Lambda}_{\pm1}$; this then implies equal spectral shifts, as claimed above.

To obtain the off-diagonal element V_{12}, we apply the same penetration-depth argument to the special case $\alpha=\pi/4$ where Eq. (2) yields the hybrid modes. Their plane-wave amplitudes $\tilde{\Psi}^{s(p)}_{N,m,1}(\theta)$ and $\tilde{\Psi}^{s(p)}_{N,m,2}(\theta)$ can be written purely in terms of the LG amplitudes $\tilde{\Lambda}^p_{\pm1}(\theta)$ using Eq. (2), and their splitting $\Delta k_{\mathrm{hybrid}}\equiv k_{N,m,2}-k_{N,m,1}$ is given by

$$\Delta k_{\mathrm{hybrid}} = -(k/L)(\delta L_{N,m,2} - \delta L_{N,m,1}) \tag{6}$$

$$= \frac{\epsilon_p-\epsilon_s}{L}\int \theta^3\tilde{\Lambda}^p_{+1}(\theta)\tilde{\Lambda}^p_{-1}(\theta)d\theta, \tag{7}$$

where k is the unperturbed wave number. Therefore, we reach $|\Delta k_{\mathrm{hybrid}}|\gg|\Delta k_{\mathrm{LG}}|$ if the form birefringence quantity $|\epsilon_p-\epsilon_s|$ is made large. On the other hand, $\alpha\to\pi/4$ implies $|V_{12}|\gg|V_{22}|$, so that the eigenvalues of V in this limit are $\delta k_{1(2)}\approx\mp V_{12}$. Setting $2\delta k_2$ equal to Eq. (7) and performing the θ integral, one obtains

$$V_{12} = V_{21} = \frac{\epsilon_p(k)-\epsilon_s(k)}{8}\sqrt{(N+1)^2-m^2}\frac{\theta_{\mathrm{D}}^2}{L}. \tag{8}$$

For some simple dielectric mirrors, $\epsilon_p-\epsilon_s$ may be swept across zero by varying the cavity length across the nominal L at which the mode pair of interest has unperturbed k equal to the design (center) wave number of the mirror, k_d. The mixing angle α can be written as

$$\alpha = (1/2)\arctan\{[\epsilon_p(k)-\epsilon_s(k)]/\Delta\epsilon\}, \tag{9}$$

where the width of the crossover interval is given by

$$\Delta\epsilon(L/R,N,m) = \frac{m}{2}\sqrt{\frac{(L/R)(1-L/R)}{(N+1)^2-m^2}}. \tag{10}$$

The formulas above complete the lowest-order degenerate perturbation theory for paraxial-mode mixing. Interestingly, $\Delta\epsilon$ is *independent of wavelength*: for fixed cavity geometry and mode labels N and m, modes of different longitudinal node number (along $\hat{\mathbf{z}}$) will have different k but identical anticrossing behavior when α is plotted versus $\epsilon_p-\epsilon_s$. This universal functional form provides a robust way of tailoring any desired mixing angle α. Most importantly, under the aspect of OAM nonconservation, we can tune Eq. (2) to $\alpha=0$.

Once the cavity linewidth for the relevant paraxial modes becomes less than the mode separation, $\Delta k\equiv2\delta k_2 \geqslant m/(4kLR)$, the two modes $\boldsymbol{\Psi}_{N,m,j}$ given by Eqs. (2), (9), and (10) are resolved at slightly different k (or L). Any excitation of the cavity would generally have nonzero overlap with these modes, and thus complicated mode patterns [5,13] can be generated by simple excitation. The magnitude of α is zeroth order in θ_{D}^2, and excursions near the asymptotic values can be seen in Fig. 1(c). The magnitude of the relative frequency splitting, however, is $O(\theta_{\mathrm{D}}^4)$ as $\theta_{\mathrm{D}}\to0$. We note that observed modes will not be restricted to $m\geqslant0$. Axial symmetry creates an exact twofold degeneracy of the vectorial LG basis modes under the transformation in which m, ℓ, and s switch sign [10]. The presence of the exact degeneracy[2] does not "wash out" the generation of complicated mode patterns and is more fully discussed in Refs. [10,13,15].

We have numerically calculated modes for $R=100$ μm and $L=2.5-25$ μm with a DBR comprising 36 pairs of quarter-wave dielectric layers A and B with refractive indices $n_A=3.52$ and $n_B=3.00$, with layer B at the top surface. Typical values of $\epsilon_{s(p)}$ were around -3, with $d(\epsilon_p-\epsilon_s)/d(k-k_d)\approx-2.8$ μm. Data were analyzed for modes close to $\lambda_d\equiv2\pi/k_d\approx400$ and 800 nm. We considered mode pairs with $N=2$ and $m=1$, the lowest values for which OAM mixing can occur.

The numerical data for the mixing angle are fit extremely well by Eq. (9) if we allow for an offset b in the argument of the arctan, as done in Fig. 1(c). The comparison between the numerical fit and Eq. (10) is shown in Fig. 2. The offset b has median -0.32 for our data and empirically behaves as $C/[kL(1-L/R)]$, where C is a slowly varying function of k

[2]This results in a degenerate (superimposable) SU(2) sector which externally multiplies the nondegenerate (mixable) SU(2) sector we have considered in Eq. (2). The location, or "generalized polarization," of each observed mode within the exactly degenerate sector is excitation dependent, while the cavity fixes the location (α) within the mixable sector.

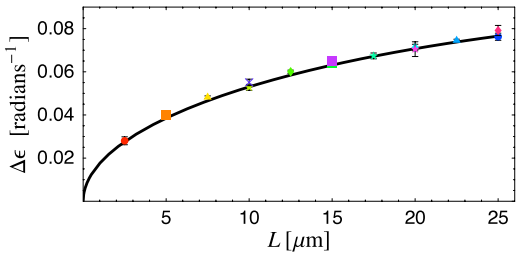

FIG. 2. (Color online) Mode-coupling width $\Delta\epsilon$ from fit (symbols) compared to perturbative prediction (solid line), plotted as a function of the cavity length L at fixed $R=100$ μm. Error bars were obtained from the fits of Fig. 1(c). Because the analytic equation (10) is wavelength independent, all data for $\lambda \approx 400$ nm and $\lambda \approx 800$ nm fall onto the same curve.

and k_d. Taking the limit $\theta_D \to 0$ such that L/R is bounded away from 0 and 1 implies that $|b|=O(\theta_D^2)$. This next-highest-order correction to our perturbation theory will be discussed in a subsequent publication [15].

To spectrally resolve the transverse mode splitting along the entire mixing curve, the cavity must obey $2kR[1-(R_1R_2)^{1/2}]<m$, where $R_{1(2)}$ are the power reflectivities of the two mirrors. Microwave experiments may be the most direct approach. Alternatively, paraxial spin-orbit coupling may be realized in microcavity resonators for quantum-information applications (cf. Ref. [12]), where small size and high finesse are required. Such cavities could generate OAM or hybrid beams at light levels from single-photon-on-demand to that of a macroscopic laser. In particular, one could utilize the fine structure and varied spatial patterns of the split modes. This has particular potential for quantum-information applications: the order-N family provides $N+1$ nearly degenerate energy levels corresponding to modes having different vectorial spatial patterns of the electric field. This spectral and spatial structure combined with quantum dots at the planar mirror may possess quantum logic capability.

In conclusion, both the mixing angle and the frequency splitting for OAM–mixed paraxial resonator modes in an axisymmetric cavity have been analytically derived here in a degenerate perturbation theory which includes the form birefringence of a practical mirror. The phenomenon is similar in principle to the polarization coupling observed in Refs. [9,16]: differences in the penetration depths for TE and TM plane waves modify the vectorial resonator modes. For our case, however, eigenmode coupling persists from the non-paraxial regime to the deeply paraxial regime. By examining the latter, we have shown here that the coupling can in fact be turned on and off via the material parameters $\epsilon_{s(p)}$. The underlying inadequacy of a scalar paraxial treatment is washed out in macroscopic cavities, but must be regarded as a fundamental limitation in high-finesse microcavities, where the correct starting point for any paraxial formulation must be the mode basis of Eq. (2), which is heterogeneous in orbital angular momentum.

This work is supported in part by National Science Foundation Grant No. ECS-0239332.

[1] L. Allen *et al.*, in *Progress in Optics*, edited by E. Wolf (Elsevier, Amsterdam, 1999), Vol. 39, pp. 291–372.
[2] O. Hosten and P. Kwiat, Science **319**, 787 (2008).
[3] R. Loudon, Phys. Rev. A **68**, 013806 (2003).
[4] A. V. Dooghin, N. D. Kundikova, V. S. Liberman, and B. Y. Zeldovich, Phys. Rev. A **45**, 8204 (1992).
[5] D. H. Foster and J. U. Nöckel, Opt. Lett. **29**, 2788 (2004).
[6] K. Y. Bliokh and D. Y. Frolov, Opt. Commun. **250**, 321 (2005).
[7] P. K. Yu and K. Luk, IEEE Trans. Microwave Theory Tech. **32**, 641 (1984).
[8] J. U. Nöckel, Opt. Express **15**, 5761 (2007).
[9] I. V. Babushkin, M. Schulz-Ruhtenberg, N. A. Loiko, K. F. Huang, and T. Ackemann, Phys. Rev. Lett. **100**, 213901 (2008).
[10] D. H. Foster and J. U. Nöckel, Opt. Commun. **234**, 351 (2004).
[11] C. W. Erickson, IEEE Trans. Microwave Theory Tech. **23**, 218 (1975).
[12] G. Cui *et al.*, Opt. Express **14**, 2289 (2006).
[13] D. H. Foster, Ph.D. thesis, University of Oregon, 2006, http://hdl.handle.net/1794/3778.
[14] D. H. Foster, A. K. Cook, and J. U. Nöckel, Opt. Lett. **32**, 1764 (2007).
[15] J. U. Nöckel, D. H. Foster, and A. K. Cook (unpublished).
[16] L. Fratta *et al.*, Phys. Rev. A **64**, 031803(R) (2001).